Mon. Not. R. Astron. Soc. **292,** 86–104 (1997)

The WC10 central stars CPD–56°8032 and He 2–113 – I. Distances and nebular parameters

Orsola De Marco, M. J. Barlow and P. J. Storey

Department of Physics and Astronomy, University College London, Gower Street, London WC1E 6BT

Accepted 1997 July 9. Received 1997 May 29; in original form 1996 December 30

ABSTRACT

We present the results of an analysis of the WC10 central stars CPD – 56°8032 and He 2–113 and of their surrounding planetary nebulae (PNe). UCL Echelle Spectrograph spectra with a resolving power of $R = 50\,000$, covering the wavelength range 3600–9500 Å, were obtained for both objects.

Expansion and radial velocities are derived from the nebular Balmer lines. Reddenings were derived from the observed Hα/Hβ decrements, as well as from the ratio of the radio free–free and Hβ fluxes. We find that $E(B-V) = 0.68$ for CPD – 56°8032 and 1.00 for He 2–113. The bolometric luminosity is found to be $2820\,D^2$ (kpc) $L_\odot$ for CPD – 56°8032 and $2290\,D^2$ (kpc) $L_\odot$ for He 2–113. We have used a calibration based on Magellanic Cloud Wolf–Rayet central stars to estimate a distance of 1.35 kpc to CPD – 56°8032 and 1.50 kpc to He 2–113. A comparison of the radial velocities of interstellar Na I D-line absorption components with Galactic rotation curve predictions for each line of sight yields distances which agree within the uncertainties with these values.

We also present deconvolved pre-COSTAR *HST* Hβ images, from which we derive nebular angular sizes of 1.6×2.1 arcsec^2 for CPD – 56°8032 and 1.4×1.1 arcsec^2 for He 2–113. From our spectra, nebular electron temperatures of 8800 and 8400 K are derived for CPD – 56°8032 and He 2–113 respectively, while an electron density of 6×10^4 cm^{-3} is determined for both nebulae. Sulphur is found to have a near-solar abundance in both nebulae, and the nebular nitrogen abundances are also close to solar. The nebular C/O abundance ratios (determined with the help of low-resolution *IUE* spectra) are found to be equal to 13 for CPD – 56°8032 and 10 for He 2–113, respectively, significantly higher than the values normally found for Galactic PNe. We find no detectable amounts of hydrogen in either stellar wind.

Key words: stars: individual: CPD – 56°8032 – stars: individual: He 2–113 – stars: Wolf–Rayet – planetary nebulae: general.

1 INTRODUCTION

CPD – 56°8032 and He 2–113 are the two brightest members of a class of cool Wolf–Rayet (WR) central stars of planetary nebulae (PNe), of which there are only three other confirmed examples at present [M 4–18, K 2–16 and IRAS 17514 – 1555 (PM 1–188)]. These WC10 stars have no hydrogen and may be the precursors to the hot non-radially pulsating PG1159 stars (Barlow & Storey 1993; Leuenhagen, Heber & Jeffery 1994). This link can be confirmed if one can show that the He, C and O abundances in their winds are the same as have been derived for the photospheres of PG1159 stars. They may also be the precursors of the hydrogen-deficient DB white dwarfs.

The wind expansion velocities of these WC10 stars (200 km s^{-1}) are much lower than those of most WR stars (which are > 1000 km s^{-1}). The reduced line blending means that elemental abundances can be derived more accurately than for other WR stars. The wind electron temperatures can even be derived, using dielectronic lines – allowing the first direct measurement of the temperature of a hot star wind (De Marco, Storey & Barlow 1997, hereafter Paper III).

The PNe around these two stars are two of the brightest infrared emitters known amongst PNe (as revealed by the

near-infrared photometry of Webster & Glass 1974 and the mid-infrared photometry of Cohen & Barlow 1980). The rich mid-infrared UIR-band spectrum of both objects was revealed by the spectrophotometry of Aitken et al. (1980) and Cohen et al. (1989). Very strong UIR bands are normally attributed to aromatic hydrocarbons such as PAHs. They are correlated with a high C/O ratio and indicate carbon-rich dust to be predominant (Barlow 1983; Cohen et al. 1989). Cohen et al. (1986, 1989) found that the ratio of UIR-band flux to total infrared flux was the highest in their sample. Together with the other objects in their sample, they showed a strong correlation between the UIR flux ratio and nebular C/O ratio, and Cohen et al. (1989) noted that a determination of the nebular C/O ratio for CPD – 56°8032 and He 2–113, expected to be high, was important for confirming the correlation and for throwing light on the origin of the UIR bands. We have determined the accurate nebular C/O ratios that are needed. The analysis of *IUE* spectrophotometry has shown CPD – 56°8032 to possess an abnormal ultraviolet (UV) reddening law, with an unusually weak 2200-Å extinction feature (Rao, Giridhar & Nandy 1990; Jeffery 1995), consistent with a significant fraction of the extinction to the star arising from circumstellar dust.

CPD – 56°8032 was first recognized as a cool carbon WR star by Bidelman, MacConnel & Bond (19689), while He 2–113 was found to be an emission-line star by Henize (1967; the spectrum was later discussed by Carlson & Henize 1979). Cowley & Hiltner (1969) described an intermediate-dispersion spectrum of the blue spectral region of CPD – 56°8032, and found weak nebular hydrogen and forbidden lines which were much narrower than the stellar He I, C II, C III and O II emission lines. They measured $V=11.04$ and estimated an $E(B-V)$ of 0.44. Thackeray (1977) described the red region of CPD – 56°8032's spectrum, observed at intermediate resolution. Webster & Glass (1974) noted that both CPD – 56°8032 and He 2–113 (as well as M 4–18 and V 348 Sgr) had spectra in which C II lines dominated those of C III, implying spectral types later than WC9, the latest that had then been defined for massive WC Wolf–Rayet stars. They proposed a new spectral type, WC10, for the first three stars, and WC11 for V 348 Sgr. The presence of narrow nebular hydrogen and forbidden lines in their spectra led Webster & Glass to classify the stars as cool WC10 central stars of PNe. Carlson & Henize (1979) later reclassified all these central stars as WC11, instead calling the nucleus of SwSt 1 (HD 167362) a WC10 star. However, it has been argued elsewhere that it is inappropriate to label SwSt 1's nucleus as a WC10 star (Mendez 1982; Tylenda, Acker & Stenholm 1993; Crowther, De Marco & Barlow 1997), and that CPD – 56°8032 and He 2–113 should therefore revert to the original classification of WC10 given by Webster & Glass.

The nebular properties of CPD – 56°8032 were investigated by Houziaux & Heck (1982), who derived the nebular carbon abundance, while Rao (1987) derived abundances of nitrogen, oxygen and sulphur for both CPD – 56°8032 and He 2–113. Cohen et al. (1989) studied the C/O ratio in both nebulae.

Pollacco et al. (1992) discovered CPD – 56°8032 to be a variable star, showing two symmetric minima in its light curve about a year apart, both with a duration of about 10 d. Lawson & Jones (1992) published further photometry of the star, covering a time-span of about 1600 d. They found that the decline time from the mean visual magnitude of 11.1 to the minimum magnitude of 12.4 was about 80 d, with the initial fade occurring particularly quickly, in about 10 d. They estimated the typical recovery time to be about 400 d. Lawson & Jones (1996) found that outside of the deep minima there appears to be a regular variation with an amplitude of 0.4 mag and a period of 125 d. The deep minima exhibited by CPD – 56°8032 suggest parallels with the hydrogen-deficient RCrB stars, whose deep declines are attributed to obscuration events by ejected dust clumps (e.g. Clayton 1996). However, He 2–113 (a spectroscopic twin to CPD – 56°8032) has been monitored at visual wavelengths over a period of 5 yr by Lawson & Jones (private communication), and was found not to vary within the observational uncertainties of ± 0.1 mag.

In Section 2 of this paper, we describe our own spectroscopic data, give details of the data reduction methods, and summarize the revised classification scheme for the [WCL] central stars. In Section 3, the nebular Balmer lines ratios are discussed and reddenings, broad-band stellar magnitudes, and the radial and expansion velocities of the nebulae are derived. In Section 4, the distance to the objects are estimated. In Section 5, pre-COSTAR *HST* Hβ images of the nebulae around the two stars are analysed for the first time. In Section 6, electron temperatures and densities are determined for both nebulae, together with nebular abundances for carbon, oxygen, nitrogen and sulphur, relative to hydrogen. Finally, in Section 7, we draw some conclusions.

2 OBSERVATIONS AND DATA REDUCTION

2.1 UCL Echelle Spectrograph spectra of CPD – 56°8032 and He 2–113

CPD – 56°8032 and He 2–113 were observed with the 3.9-m Anglo-Australian Telescope (AAT) on 1993 May 14 and 15 using the 31.6 line mm^{-1} grating of the UCL Echelle Spectrograph (UCLES), with a 1024×1024 pixel Tektronix CCD as detector. Four settings of the CCD were needed in order to cover the entire echellogram: two adjacent ones in the far-red and two in the blue. Complete wavelength coverage was obtained from 3600 to 9500 Å. At each wavelength setting we obtained 5-arcsec-wide-slit spectra, for absolute spectrophotometry, and 1.5-arcsec-narrow-slit spectra, for maximum resolution ($R=50\,000$). The continuum signal-to-noise ratios ranged from 20 to 60, depending on exposure time and the brightness of the object. A log of the observations is presented in Table 1.

The data were reduced using the IRAF (v2.10) package[1] at the UCL Starlink node. Wavelength calibration was with respect to comparison Th-Ar arc exposures, and absolute flux calibration was with respect to the B3IV star HD 60753, whose energy distribution has been measured by Oke (1974, 1990). The flux calibration was achieved by first flat-fielding, background-subtracting and wavelength-calibrating the spectrum of HD 60753. Next, a comparison was made between the counts in every wavelength bin (of 2-Å width) and the tabulated Oke fluxes in that bin. This was achieved

[1]IRAF is written and supported by the national Optical Astronomy Observatories (NOAO) in Tucson, Arizona. http://iraf.noao.edu/

Table 1. Log of the 1993 UCLES observations. Only the second night was photometric.

Star	Run	Central wavelength (Å)	Date 1993, May	Exposure time (sec)	Slit width (arcsec)	Airmass	Seeing (arcsec)
He 2–113	102	4622	14	500	1.5	1.71	2
	105	4622	14	600	1.5	1.60	2
	107	4622	14	600	1.5	1.54	2
	123	4622	14	600	1.5	1.08	4
	125	4622	14	600	1.5	1.09	4
	176	6827	15	600	5.0	1.67	2
	178	6960	15	600	5.0	1.59	2
	180	4622	15	400	5.0	1.54	2
	236	6827	15	1200	1.5	1.29	2
	239	6960	15	1200	1.5	1.40	2
CPD–56°8032	120	4622	14	600	1.5	1.28	4
	121	4622	14	600	1.5	1.25	4
	122	4622	14	600	1.5	1.23	4
	133	4622	14	300	5.0	1.11	2.5
	134	4622	14	300	5.0	1.11	2.5
	204	6827	15	500	5.0	1.42	1.5
	206	6960	15	500	5.0	1.39	1.5
	241	6960	15	1200	1.5	1.19	2
	242	6827	15	1200	1.5	1.23	2

by locating about 30 points per order on the continuum of the standard star, and fitting them to a polynomial in wavelength, allowing the creation of a calibration curve (counts versus flux units) for every order of the standard spectrum. This curve was then applied to the target star to convert counts to flux units.

Care was needed to create a calibration curve free of glitches. Misfittings of the echelle orders could occur if the order of the fitting polynomial was too high; conversely, a low-order polynomial could miss real flux changes. The join between successive orders was a measure of how successful the flux calibration had been.

The echelle orders were then merged to produce a continuous spectrum extending from 3600 to 9500 Å. Subsequent data reduction was carried out with the Starlink DIPSO package (Howarth & Murray 1988), particularly heavy use being made of the ELF suite of emission-line fitting subroutines, written by one of us (PJS).

After flux calibration, the narrow-slit spectra were scaled up to the continuum levels of the wide-slit spectra. For CPD – 56°8032, the blue spectra were obtained during the second half of the first night, which was not photometric. In order to scale the blue part of its spectrum to the correct level, we calculated a 'scaling' factor from the flux in the nebular hydrogen lines. This was done by taking the ratio between the measured Hβ flux and that measured from a wide-slit spectrum taken in photometric conditions in 1981 by us (see below). The scaling factor was 1.42 ± 0.04. After this factor was applied to the blue spectrum, the alignment with the red part was almost perfect.[2]

[2]Despite the blue part of our 1993 CPD – 56°8032 spectrum having been scaled to the 1981 spectrum, the values of the Hβ fluxes listed in Table 4 for the two spectra differ by about 5 per cent. This is due to a subsequent remeasuring of the 1993 Hβ flux. However, the new value is within the errors associated with flux measurements, and is not considered to be a cause of concern.

Neither of the two echelle spectra is displayed here in their entirety, but they are presented, together with complete line identifications, by De Marco et al. (in preparation).

2.2 RGO Spectrograph spectrum of CPD – 56°8032

On 1981 July 22, a spectrum of CPD – 56°8032 was taken with the 3.9-m AAT using the RGO Spectrograph 25-cm camera with an IPCS as detector. A log of the observations is presented in Table 2. A 1200 line mm^{-1} grating, blazed in the red, was used in first order to acquire spectra longwards of 5000 Å at a dispersion of 33 Å mm^{-1}, and was used in second order to obtain spectra shortwards of 5000 Å at a dispersion of 16 Å mm^{-1}. Appropriate order-sorting filters were used. The wavelength coverage per spectrum was about 1000 and 500 Å in first and second order respectively. When using a narrow slit (1.0–1.5 arcsec), the instrumental resolution, as judged from the FWHM of comparison arc lines, was typically 0.98 and 0.50 Å, in first and second order (the instrumental resolution was lower, though, at the edges of the detector field). With a wide slit (8.3 arcsec), the instrumental resolution was 3.0 and 1.5 Å in first and second order respectively.

Spectra were obtained at eight different grating settings, yielding complete wavelength coverage between 3600 and 8700 Å, with the wavelength overlaps between adjacent spectra being typically about 120 Å. At each wavelength setting, narrow-slit spectra (for maximum resolution) and wide-slit spectra (for absolute spectrophotometry) were obtained. The data were reduced using the AAO SDRSYS package, written by J. Straede. Wavelength calibration was with respect to comparison Cu-Ar arc exposures, and absolute flux calibration was with respect to the DA white dwarf W485A, whose energy distribution has been measured by Oke (1974). Subsequent data analysis was also

Table 2. Log of the 1981 July 22 RGO spectrograph observations of CPD – 56°8032.

Run	Starting wavelength (Å)	End wavelength (Å)	Exposure time (sec)	Slit width (arcsec)	ND Filter[a] (dex)
32,34	5007	5968	500,500	0.7	none,0.7
36,37	5007	5968	450,200	0.7	0.7,1.3
40,41,42	5850	6811	500,320,200	0.8	none,1.0,0.34
44,45	5850	6811	300,200	8.3	0.7,1.3
46,47,48	6773	7723	240,100,150	8.3	0.34,1.3,0.7
50,51,52	6773	7723	500,180,80	1.2	none,0.7,1.0
55	7748	8698	1000	3.5	none
57	7748	8698	400	8.3	none
59	3325	3805	900	1.5	none
62	3325	3805	321	8.3	0.34
63,64	3775	4255	300,100	8.3	0.7,1.0
66,67	3775	4255	650,120	1.5	0.34,0.7
70,71	4247	4727	650,120	1.5	0.34,1.0
73,74	4247	4727	100,250	8.3	1.0,0.7
75,76	4591	5050	250,120	8.3	0.34,0.7
78,79,80	4591	5050	200,400,100	1.5	none,0.34,0.7

[a]The neutral-density filters were introduced to reduce the count rates so that the strongest lines would not saturate.

carried out within the Starlink DIPSO package (Howarth & Murray 1988).

After flux calibration, the narrow-slit spectra were scaled up to the continuum levels of the wide-slit spectra. Regions where strong emission lines had caused detector saturation were replaced by the equivalent regions from spectra, obtained immediately adjacent in time, which used a neutral-density filter to reduce the count rate. Finally, the resulting absolutely calibrated narrow-slit spectra were merged to produce a continuous spectrum extending over 14 000 pixels from 3600 to 8700 Å.

2.3 Classification of CPD – 56°8032 and He 2–113

Some disagreement over the classification of [WCL] CSPN has been evident in the literature. Webster & Glass (1974) noted that the nuclei of CPD – 56°8032, He 2–113, M 4–18 and V 348 Sgr all had spectra in which C II emission lines dominated those of C III, implying spectral types later than WC9, the latest that had then been defined for massive WC Wolf–Rayet stars by Smith (1968). Carlson & Henize (1979) noted that Swings & Struve (1940) had found the nucleus of SwSt 1 (HD 167362) to have a lower excitation spectrum than any other WC star then known, and that they had classified it as one class later than stars now known as WC9. Carlson & Henize therefore classified the nucleus of SwSt 1 as WC10 and inferred still later types for the four stars discussed by Webster & Glass, though not explicitly introducing a WC11 class. In their table IX, van der Hucht et al. (1981) classified the nucleus of SwSt 1 as WC10, and classified the four nuclei discussed by Webster & Glass as WC11.

However, if the spectrum of SwSt 1 is compared with those of CPD – 56°8032 and He 2–113 or with those of other WC10, WC9 and WC8 stars, it is clear that SwSt 1 does not belong to the WC class at all and is better classified as a weak emission-line star (Tylenda et al. 1993; see also Mendez 1982). Crowther et al. (1997) present spectra of a set of [WCL] stars, as well as SwSt 1. They show that the criteria for the classification of massive WC stars, adopted also for the WC central stars of PNe, are not appropriate for stars like HD 167362. The elimination of SwSt 1 from the [WCL] sequence leaves CPD – 56°8032 and He 2–113 as WC10 stars; other WC10 central stars then include M 4–18, IRAS 17514 – 1555 (PN PM 1–188, HuBi 1) and IRAS 07027 – 7934, while K 2–16 is found to be the current sole representative of the WC11 class (Crowther et al. 1997).

3 APPARENT MAGNITUDES, RADIAL VELOCITIES AND REDDENINGS

3.1 Apparent magnitudes

We convolved our observed spectra of CPD – 56°8032 and He 2–113 with broad-band V and B filter profiles (kindly made available to us by J. R. Deacon) to obtain an estimate of the apparent V and B magnitudes of the stars. For CPD – 56°8032, the V magnitude in 1993 May was found to be 10.9 ± 0.1, indicating that the star was at maximum light and in agreement with the estimate of W. Lawson and A. Jones (private communication) of 11.0 ± 0.1 for the same epoch. The B magnitude derived from our 1993 spectrophotometry is 11.25 ± 0.1. Lawson and Jones's light curve for CPD – 56°8032, sampled between JD 244 7200 (early 1988) and 245 0300 (1996 October), indicated that during this period the star had two declines, each followed by a recovery to maximum light ($V \sim 11.0$): one starting in 1990 March and one in 1994 August. The star took about 400 d to recover fully from the first minimum, which had an initial depth of about 1.3 mag. From our 1981 spectrum of CPD – 56°8032 we derive a V magnitude of 11.01 ± 0.1 and a B magnitude of 11.38 ± 0.1, again indicating that the star

was at maximum light. For He 2–113, we derive $V=11.7\pm0.1$ and $B=12.3\pm0.1$ in 1993 May. W. Lawson and A. Jones (private communication) found that He 2–113 never varied from a mean magnitude of $V=12.0\pm0.1$ since 1990 late September.

3.2 The nebular Balmer lines in the spectra of CPD – 56°8032 and He 2–113

The Hα and Hβ lines observed in the spectra of both CPD – 56°8032 and He 2–113 have shapes that cannot be perfectly fitted with a single Gaussian. This could indicate either the presence of an underlying stellar component or that the nebula has an irregular velocity structure.

The main argument in favour of a nebular origin for the entire flux in the Balmer lines comes from a comparison of the Hα line profiles with those of the nebular [O I] line at 6300 Å (see Fig. 1). As can be seen, the widths and the overall shapes of the wings of the lines are very similar. A comparison of the Hβ profiles with those of the circumnebular sodium D lines seen in absorption in the spectra of both stars also supports a nebular origin for the broad wings (see Section 3.4 and Fig. 2). The lack of evidence for Balmer line emission from the stellar winds is discussed further by De Marco & Crowther (1997, hereafter Paper II). The observed Hα and Hβ line fluxes from both nebulae are presented in Table 4.

3.3 Nebular radial velocities and expansion velocities from the Balmer lines

Radial velocities for the nebulae were obtained by determining the wavelength shifts of the nebular Balmer lines (the Hα and Hβ lines were used, since Hγ and Hδ were blended with stellar features, but a check using Hγ and Hδ did not show any serious discrepancies). The shift was determined by fitting a single Gaussian to each of the Hα and Hβ lines. Although a single Gaussian did not fit the profiles very well, it was felt that it was the best way to locate the overall centre of weight of the line without introducing biases due to the asymmetry of the nebular lines. Mean heliocentric radial velocities of -59.4 ± 3.0 and -57.3 ± 3.0 km s^{-1} were found for CPD – 56°8032 and He 2–113 respectively, corresponding to LSR radial velocities of -59.6 and -58.4 km s^{-1} respectively. These radial velocities are listed in Table 3, together with the nebular expansion velocities, which were assumed to be given by the mean half-width at half-maximum of the Hα and Hβ line profiles. Sahai, Wootten & Clegg (1993) have measured the LSR radial velocity of CPD – 56°8032 in the CO $J=2$–1 and 1–0 lines, and list a value of -57 km s^{-1} for both CO lines (no uncertainty quoted), which agrees with the value of (-59.6 ± 3.0) km s^{-1} found here from the nebular Balmer lines. Sahai et al. (1993) also determined a FWHM of 50 km s^{-1} for the $J=1$–0 and 2–1 CO lines, in reasonable agreement with the mean FWHM of 60 km s^{-1} derived here for the Hα and Hβ lines, which we assume to be equal to twice the nebular expansion velocity.

3.4 High-velocity components in the circumstellar neutral gas

In Appendix B the sodium D lines are used to obtain an estimate of the distance to CPD – 56°8032 and He 2–113. There we argue that some of the sodium D-line radial velocity components are of nebular origin. However, a question which remains to be addressed is the origin of the highest velocity components of the sodium D lines. If their origin is nebular, we would expect to find the absorption features at a velocity corresponding to the radial velocity of the star minus the nebular expansion velocity. From the nebular LSR radial velocities and expansion velocities listed in Table 3, we would then expect a velocity component at -90 km s^{-1} for CPD – 56°8032, and one at -77 km s^{-1} for He

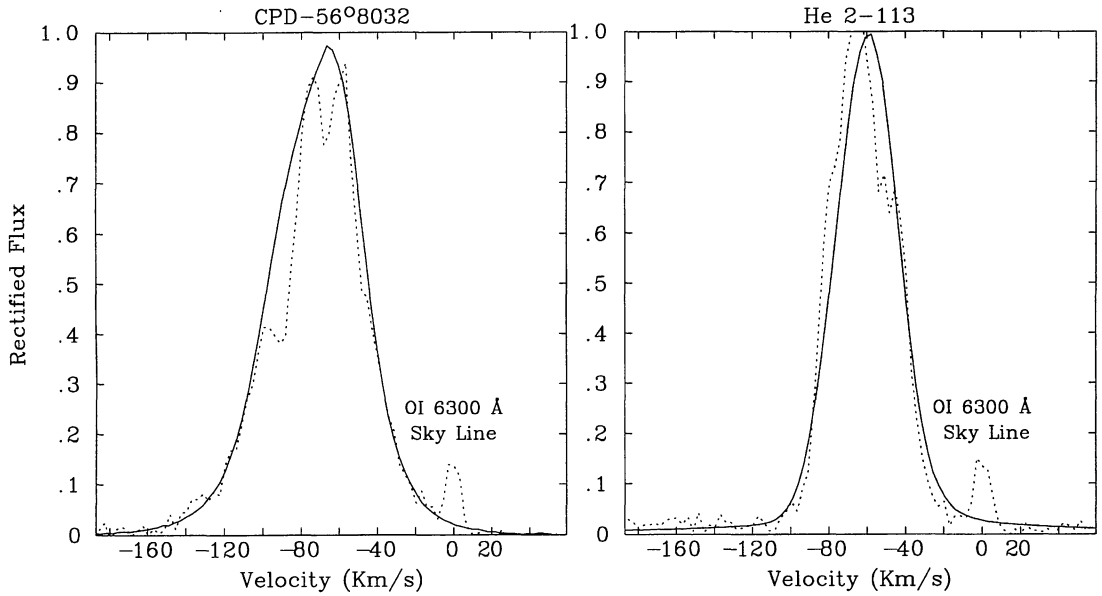

Figure 1. Comparison of the Hα line profile (solid) with that of the nebular [O I] line at 6300 Å (dotted), for CPD – 56°8032 (left) and He 2–113 (right).

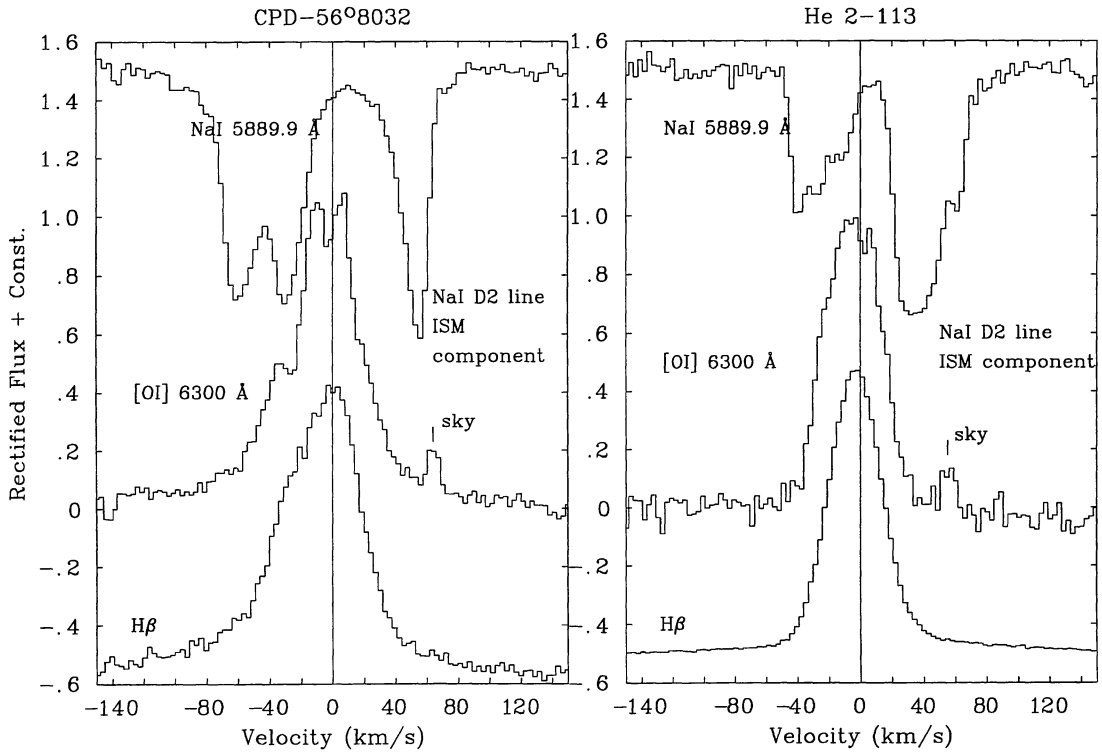

Figure 2. Comparison of the sodium D2 line profile (upper), the nebular [O I] line profile at 6300.3 Å (middle), and the Hβ line profile (lower) for CPD – 56°8032 (left) and He 2–113 (right). All velocities are corrected to zero-points corresponding to the radial velocities of the nebulae.

Table 3. Radial velocities derived for the components of the sodium D line velocity components. The nebular expansion velocities are derived from an average of half the FWHM of the Hα and Hβ lines.

Star's Name	LSR Radial Velocity (km s^{-1})	Nebular expansion Velocity (km s^{-1})	LSR R.V. of Components (km s^{-1})	D (kpc) (rotation curve)	$\|z\|$ (pc)	D (kpc) (IR flux)
CPD–56°8032	–59.6 ± 3.0	30 ± 4	–124 –110 –93 –20 –15 –7	1.6 ± 0.2	275	1.35 ± 0.3
He 2–113	–58.4 ± 3.0	19 ± 1	–97 –85 –68 –28 –19 0 +4	1.9 ± 0.2	132	1.50 ± 0.3

Table 4. Fluxes measured for the nebular hydrogen lines.

Star	Line	1993 Flux (ergs cm^{-2} s^{-1})	1981 Flux (ergs cm^{-2} s^{-1})	1978/79 Flux (Aitken et al., 1980) (ergs cm^{-2} s^{-1})
CPD–56°8032	Hα	3.98×10^{-12}	5.38×10^{-12}	6.31×10^{-12}
	Hβ	9.60×10^{-13}	9.23×10^{-13}	1.12×10^{-12}
He 2-113	Hα	1.75×10^{-11}	–	–
	Hβ	2.16×10^{-12}	–	1.51×10^{-12}

2–113. We identify these with the Na I components observed at -93 km s^{-1} (i.e., -33 km s^{-1} relative to the nebular central velocity) for CPD – 56°8032 and at -85 km s^{-1} (i.e., -27 km s^{-1} relative to the nebular central velocity) for He 2–113 (Fig. 2; the combined error on the LSR radial velocity and on the nebular expansion velocity, together with the likely error on the velocity shift of the sodium D-line components, ± 5 km s^{-1}, can explain the differences). In addition, each nebula shows further Na I absorption components with even greater blue shifts, at LSR velocities of -110 and -124 km s^{-1} in the case of CPD – 56°8032 (i.e., at -50 and -74 km s^{-1} in the nebular velocity frame) and at -97 km s^{-1} in the case of He 2–113 (-38 km s^{-1} in the nebular velocity frame).

An alternative way to look for a confirmation of the presence of high-velocity nebular components is to look at the structure of nebular lines that should be formed in a similar region to the neutral sodium. Lines with this characteristic are, for instance, the [O I] $\lambda\lambda$6300.3, 6363.8 doublet (the higher energy of the upper level of the 5577-Å line makes it more difficult to excite, and only the sky counterpart was present in the spectrum). In Fig. 2, the profile of

[O I] λ6300 is plotted, along with that of the sodium D2 line. On the *y* axis we plot the rectified profiles, offset by arbitrary constants. On the *x* axis, the zero-point corresponds to the nebular radial velocity. If we ignore anything with a velocity more positive than the nebular velocity (i.e., the interstellar component of the sodium D2 line, the sky component of the [O I] 6300-Å line, and the nebular [O I] emission coming from the part of the nebula receding from the observer – for obvious reasons the latter would not have a sodium absorption counterpart), we notice a certain correspondence: for CPD −56°8032 the well-defined troughs of the blueshifted Na I D2 components correspond to the extended blue wing in the [O I] line profile. We underline that the slight mismatch in Fig. 2 between the bluest [O I] component and the velocity of the Na I absorption component nearest to it is only 3.2 km s^{-1}, within the uncertainties in the respective wavelength calibrations. The same applies to He 2–113, although the most blueshifted part of the sodium D2 line component does not find a match in the [O I] line profile.

We also measured the width of the [C I] λ8728 line, which could also originate from the nebula. This line was observed in the echelle spectra of both CPD −56°8032 and He 2–113. Its FWHM, 48 km s^{-1} for CPD −56°8032 and 30 km s^{-1} for He 2–113, was somewhat smaller than the FWHM of the nebular [O I] lines.

We note that not only do the widths of the Hβ lines match the widths of the respective [O I] lines (as already demonstrated in Fig. 1, using Hα), but that this allows us finally to explain the asymmetry in the hydrogen lines, which could not be explained by the presence of a stellar wind component (the lack of stellar hydrogen is also argued in Paper II).

3.5 Reddenings

The reddening to each object can be derived by comparing the fluxes in the nebular Hα and Hβ lines (see Table 4); the weaker Hγ and Hδ lines were too blended to measure their fluxes reliably. Using the case B hydrogen recombination coefficients of Storey & Hummer (1995) for a nebula with electron density $N_e = 10^4$ cm^{-3} and electron temperature $T_e = 10^4$ K and the Galactic reddening law of Howarth (1983), values of $E(B-V)$ were derived (Table 5). The radio observations of CPD −56°8032 and He 2–113 by Purton et al. (1982) indicate an optically thin free–free spectrum between 2.7 and 14.7 GHz for CPD −56°8032, with a 5.0-GHz flux of 26 ± 4 mJy, and an optically thin free–free spectrum above about 9.0 GHz for He 2–113, with a 14.7-GHz flux of 160 ± 10 mJy. Reddenings were therefore also derived from a comparison of the radio and Hβ fluxes, using the method of Milne & Aller (1975) – the derived values of $E(B-V)$ are listed in Table 5. In Tables 4 and 5, we also list the fluxes and reddenings obtained by Aitken et al. (1980) from observations carried out in 1978 and 1979.

3.5.1 *CPD −56°8032*

The 1993 Hα–Hβ baseline yielded an $E(B-V)$ of 0.34 mag [$c(H\beta) = 0.49$], much lower than the radio–Hβ value of 0.68 mag [$c(H\beta) = 0.99$]. The 1993 spectrum of CPD −56°8032 was considered optimal in terms of resolution but, bearing in mind that the blue part was not obtained in photometric conditions and had to be rescaled as described in Section 2.1, it was decided that the Hα–Hβ baseline was the more susceptible to error, while the longer radio–Hβ baseline should smear out better the possible errors in the corrected Hβ flux. This reasoning was supported by measurements of the 1981 spectrum that yielded an $E(B-V)$ of 0.68 from the Hα–Hβ baseline and a radio–Hβ value for $E(B-V)$ of 0.69 [$c(H\beta) = 0.99$]. We finally adopted $E(B-V) = 0.68$ [$c(H\beta) = 0.99$], as given by three out of four of our 1993 and 1981 ratios. We have not used the method of nulling the 2175-Å interstellar extinction feature to estimate a value of $E(B-V)$, since the UV reddening law towards CPD −56°8032 has already been shown to be abnormal (Rao et al. 1990; Jeffery 1995; see also Section 6.1, where He 2–113 is also found to have an abnormal UV reddening law).

3.5.2 *He 2–113*

The same methods as above were used to obtain $E(B-V)$ for He 2–113. The radio–Hβ baseline yielded $E(B-V) = 1.02$ [$c(H\beta) = 1.47$], while the Hα–Hβ baseline yielded $E(B-V) = 0.98$ [$c(H\beta) = 1.41$]. The better agreement between the two baselines can be ascribed to the fact that, for this star, the entire optical spectrum was obtained in photometric conditions and no corrections were necessary. We finally adopted a value of $E(B-V) = 1.00$ [$c(H\beta) = 1.44$] for He 2–113.

4 DISTANCES

We adopt distances of 1.35 and 1.50 kpc for CPD −56°8032 and He 2–113 respectively (Table 3), as found using the infrared bolometric luminosity method described in Appendix A, and consider the rotation curve distances (described in Appendix B) of 1.6 kpc (CPD −56°8032) and 1.9 kpc (He 2–113) as confirmation that the distance to both stars is indeed between 1 and 2 kpc, and not as large as the value of 2.36 kpc obtained for CPD −56°8032 by Rao et al. (1990) using a relation between dust temperature and nebular

Table 5. Reddenings derived from Balmer line ratios and from the radio-to-Hβ ratio.

Star	Ratio	E(B-V) (1993)	E(B-V) (1981)	1978 E(B-V) (Aitken et al.,1980)
CPD–56°8032	Hα/Hβ	0.34	0.68	0.60
	radio/Hβ	0.68	0.69	0.60
He 2–113	Hα/Hβ	1.02	–	–
	radio/Hβ	0.98	–	1.10

radius, or the value of 3.5 kpc determined for He 2–113 by Le Bertre et al. (1989) from kinematical considerations.

5 *HST* IMAGES OF CPD – 56°8032 AND HE 2–113

The nebulae of CPD – 56°8032 and He 2–113 are revealed by narrow emission lines superimposed on the central star spectra, with the latter's nebular lines showing much higher contrast against the stellar spectrum. However, the nebulae are too small to have had their structures resolved in any ground-based image. The only published dimensions for either of the two nebulae are those by Kohoutek (1996), who quotes a size for the nebulosity around CPD – 56°8032 of 1.3 × 1.2 acrsec,^{2} from a ground-based image taken in Hα, and that by Roche, Allen & Bailey (1986) who quote the 3.28-μm spatial extent of CPD – 56°8032 to be 1.3 arcsec. The latter also noted the extent of the ionized region to be similar to the extent of the region producing the 3.28-μm feature.

A search of the *HST* archive revealed that four exposures had been taken for each nebula, two each in the Hβ and [O III] 5007-Å lines, with the WF/PC in PC configuration (800 × 800 pixels × 4 chips, yielding a 66 × 66 arcsec^2 field of view with 0.043 arcsec per pixel). These images were retrieved from the archive and analysed. Details of the exposures are given in Table 6.

These eight pre-COSTAR images were already calibrated by the pipeline process (for details see the *HST* Data Handbook, 1995, p. 427). In particular, the calibrated WF/PC images flagged the static and saturated bad pixels, the analogue-to-digital conversion, bias level determination and removal, pre-flash application, dark correction and flat-fielding. However, because of the *HST* spherical aberration, the images did need to be deconvolved.

The deconvolution process was carried out using both a theoretical and an observational point-spread function (PSF). The theoretical PSF was generated by the program Tiny Tim (V4.0).[3] This is used to model the PSF of the *HST*, and is usually employed for image deconvolution and other applications. The PSFs generated in this way are easy to produce, noiseless, linear and computable for a given instrument and filter. However, due to the high-frequency structure caused by the large number of optical components, the simulations never match ring for ring the observed PSF.

For this reason, the images deconvolved in this way, despite showing all the nebular features, always displayed ghosts caused by the theoretical PSF. We therefore decided to use an observed PSF to deconvolve our images. The procedure followed was to clean cosmic rays from chip 6 (the part of the image that contained the object of interest) in all eight images, using both an automatic algorithm and a manual one. Next, the field of view was further reduced to 200 × 200 pixels centred on the star to speed up the deconvolution process.

The deconvolution was carried out using the Richardson–Lucy algorithm (R–L; see Snyder 1990), using the averaged 5007-Å images to give the PSF. The very low excitation nebulae around CPD – 56°8032 and He 2–113 show no emission in the [O III] line at 5007 Å, and consequently the 5007-Å images show only the star, while the Hβ images show both star and nebula. The R–L algorithm demands that the read-out noise and the gain be specified. This is in order to model the noise characteristics of the image properly. It is important to account for read-out noise so that low-level noise spikes are not construed as significant features, and so that negative-noise deviations do not cause the iteration to diverge. For a single WF/PC exposure the canonical values for the two parameters are 13.0 (read-out noise) and 7.5 (gain) (in the case of averaging N equals exposures, the read-out noise should be multiplied by $\sqrt{N}$). In the next two sections, we discuss the resulting images in more detail.

[3]Tiny Tim is supported by the Space Telescope Science Institute. All the documentation is available from http://www.stsci.edu/ftp/software/tinytim/

Table 6. Log of *HST* WF/PC exposures of the nebulae around CPD – 56°8032 (upper) and He 2–113 (lower) (PI: Bobrowsky).

Exposure	Filter	Exposure Time(s)	Date
w11s8p01t	F487N	140	02/10/92
w11s8q01t	F487N	140	10/10/92
w11s8r01t	F502N	35	02/04/93
w11s8s01t	F502N	35	10/10/92
w11s8d01t	F487N	120	01/02/93
w11s8e01t	F487N	120	01/02/93
w11s8f01t	F502N	30	03/03/93
w11s8g01t	F502N	30	03/03/93

5.1 The nebula around CPD – 56°8032

Fig. 3(c) shows a grey-scale plot of the nebula around CPD – 56°8032. The image was obtained by averaging the two Hβ exposures (Fig. 3a) and deconvolving the result with a PSF obtained from the average of the two [O III] exposures (Fig. 3b). Deconvolutions were also tried using all the exposures independently; the result remained the same. The 60 × 60 pixel Hβ image of CPD – 56°8032 in Fig. 3(c) shows an irregular nebula of approximate dimensions 1.65 × 2.06 arcsec^2 on the sky. The image exhibits a central 'blob', within which the star is located (A). It also shows a ring-like structure peaking in intensity south and east of the star (B). It is possible to trace this ring to the north of the star, where it is much fainter. At points C and D (better shown in the contour plot in Fig. 3d) there are two intensity peaks. Between points E and F there is an almost continuous line of emission, possibly part of a larger ring. Points G and H seem isolated from the rest of the structure. The majority of the emission originates from the southern side, possibly due to dust obscuration on the northern side. Similar spatial variations in the dust obscuration are seen across the face of NGC 7027 (Walton et al. 1988). This tempts us into speculation: the nebular hydrogen lines exhibit a 'haunch' on the blue side. This means that more nebular ionized gas is observed coming towards us. If the material positioned to the north-east of the nebula (Fig. 3c) is receding and more heavily reddened, while material to the south-

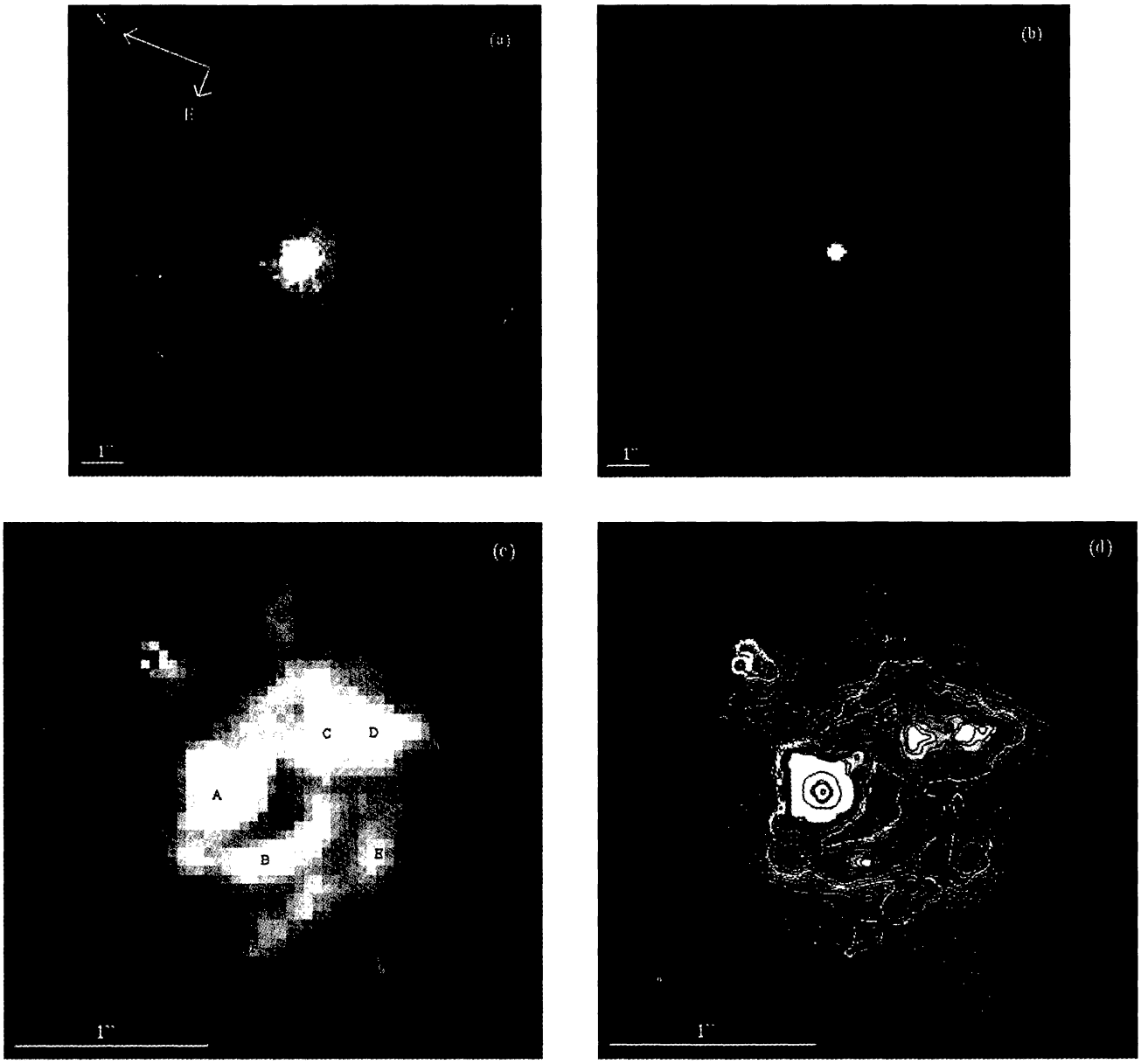

Figure 3. *HST* images of CPD – 56°8032. (a) The average of the two raw Hβ images; (b) the average of the two raw [O III] images; (c) the deconvolved Hβ image obtained using the [O III] image for the point spread function; (d) a contour map of (c); the first white contour corresponds to a level of 1 count, the last black contour corresponds to a level of 16 000 counts. The parts of the nebula labelled A–H in (c) are discussed in the text. The orientation of the images is shown in (a).

west of the nebula is approaching and less heavily reddened, this would result in the red part of the nebular lines being depressed with respect to the blue part.

Inspection of Fig. 3(c) indicates that the ring BC seems to be elongated along a north–south axis. Measurements of the radius proceeded by identifying the centre of the ring emission at different locations. The radii thus obtained were averaged to obtain major and minor radii of 0.49 and 0.38 arcsec ($\pm$0.05 arcsec) respectively. Kohoutek (1996) reported the nebular region to be 1.3×1.2 arcsec^2 from a ground-based ESO 3.6-m telescope Hα image, with the major axis oriented north–south, in reasonable agreement with the present results.

Dynamical ages obtained from *outer* nebular radii are not usually reliable, and they indicate only a lower limit to the real nebular age since the majority of the nebula is still neutral. Millimetre-wave imaging in CO, or in the continuum, would be required in order to obtain a more realistic estimate. However, inner nebular radii may give an indication of the dynamical age since leaving the AGB, since they do not suffer from this 'boundary' problem. For CPD – 56°8032's nebula it is possible to obtain such an inner radius by measuring the distance between the star and the ring-like structure. If an average of the major and minor radii (0.43 arcsec) of the ring is taken and a distance of 1.35 kpc adopted, together with a uniform expansion velocity of

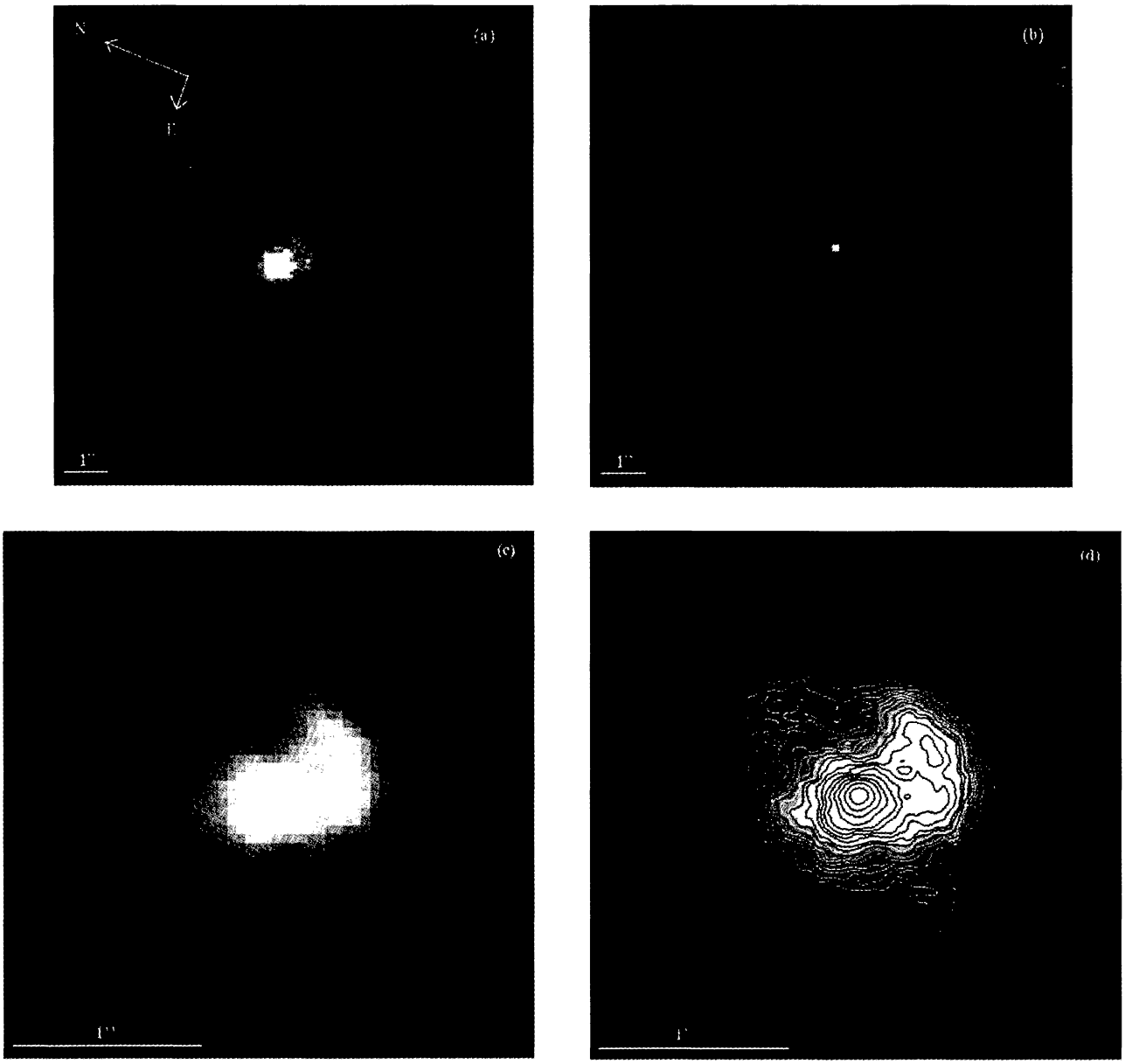

Figure 4. *HST* images of He 2–113. (a) The average of the two raw Hβ images; (b) the average of the two raw [O III] images; (c) the deconvolved Hβ image obtained using the [O III] image for the point-spread function; (d) a contour map of (c): the first white contour corresponds to a level of 1 count, the last black contour corresponds to a level of 7000 counts. The orientation of the images is shown in (a).

30 km s^{-1}, we can calculate a dynamical age of about 100 yr.

5.2 The nebula around He 2–113

The deconvolved Hβ image of this nebula is shown in Fig. 4(c), on the same scale as CPD – 56°8032. Apart from enhanced emission on the western side and, possibly, ansae along a north–south axis, very little structure is apparent in the deconvolved nebular image. We measured the nebular diameter to be about 1.4 arcsec north–south and 1.1 arcsec east–west. This, together with a distance of 1.5 kpc and an expansion velocity of 19 km s^{-1}, results in a dynamical age of about 220 yr. However, for the same reasons as given in Section 5.1, this can be only a lower limit to the age of the nebula.

6 NEBULAR ABUNDANCE ANALYSIS

6.1 Nebular line fluxes

The spectroscopic analysis of the nebulae around CPD – 56°8032 and He 2–113 is rendered difficult by the blending of nebular and stellar features. In previous analyses, Houziaux & Heck (1982) estimated the carbon abundance for the nebula of CPD – 56°8032, while Cohen et al. (1989) estimated both carbon and oxygen abundances for it (both used *IUE* data). Rao (1987) determined N/H,

Table 7. Observed (F) and dereddened (I) nebular line intensities for CPD – 56°8032, from the 1993 UCLES spectrum and from the 1981 RGO Spectrograph spectrum. The adopted reddening is $E(B-V)=0.68$. The dereddened Hβ flux as measured from the 1993 spectrum is 9.33×10^{-12} erg cm^{-2} s^{-1}; from the 1981 spectrum we find 8.97×10^{-12} erg cm^{-2} s^{-1}. Errors were assigned according to the difficulty in measuring fluxes. The unusually high FWHM of the [O I] lines are discussed in Section 4.1. The [N II] 5754.64-Å line has a low measured FWHM: this could be due to the fact that the line lies on top of a broad stellar feature (C II multiplet 21 and C III multiplet 3), making its FWHM difficult to measure accurately.

		CPD–56°8032 - 1993				CPD–56°8032 - 1981		
Ion	λ (Å)	FWHM (km s^{-1})	F (ergs cm^{-2} s^{-1})	100×I /I(Hβ)	Errors (%)	F (ergs cm^{-2} s^{-1})	100×I /I(Hβ)	Errors (%)
[O II]	3726.0	–	4.38×10^{-13}	81.8	20	3.26×10^{-13}	63.3	40
[O II]	3728.8	–	–	–	–	2.52×10^{-13}	48.9	50
Hβ	4861.3	67	9.60×10^{-13}	100	10	9.23×10^{-13}	100	5
[N II]	5754.6	45	8.61×10^{-14}	5.1	10	1.44×10^{-13}	10.0	10
[O I]	6300.3	92	3.81×10^{-13}	21.3	10	4.42×10^{-13}	25.3	10
[O I]	6363.8	80	–	–	20	–	–	–
[N II]	6548.0	67	1.26×10^{-12}	61.9	10	1.67×10^{-12}	87.8	5
Hα	6562.8	55	3.98×10^{-12}	200.4	10	5.38×10^{-12}	281.5	5
[S II]	6716.5	69	2.02×10^{-13}	9.8	10	2.03×10^{-13}	10.1	35
[S II]	6730.8	–	4.56×10^{-13}	13.9	20	5.02×10^{-13}	24.90	20
[O II]	7320	–	6.75×10^{-13}	27.6	15	7.85×10^{-13}	32.9	5
[O II]	7330	–	3.44×10^{-13}	13.9	15	6.46×10^{-13}	27.0	5
O I	8445	53	7.43×10^{-14}	2.3	10	–	–	–
[S III]	9068.9	60	8.25×10^{-14}	2.3	15	–	–	–

S/H and O/H ratios for the nebulae of CPD – 56°8032 and He 2–113, using optical spectra.

In order to distinguish the nebular lines from the stellar lines, we scanned our echelle spectra for lines having widths systematically lower than the average FWHM values for the stellar wind lines (250 km s^{-1} for CPD – 56°8032 and 160 km s^{-1} for He 2–113) and close to the FWHM widths of the nebular Balmer lines (60 and 40 km s^{-1} respectively). Once the nebular lines were identified, their fluxes were measured using the DIPSO package (Howarth & Murray 1988). The measurements were carried out on the narrow-slit spectra (for best resolution) after they had been scaled up to the wide-slit flux levels, as described in Section 2.1. The line fluxes were checked against measurements of unblended nebular lines (e.g., [S II] λ6717) in the photometric wide-slit spectra. For the lines that were blended with stellar features, deblending was attempted and the line flux assigned an error that would reflect the uncertainty in its measurement. For lines that were either too heavily blended or had low signal-to-noise ratios, the measurement was not attempted. In Tables 7 and 8 we present the nebular line fluxes for all the lines that were measured. Table 7 presents, along with measurements from the 1993 UCLES spectrum, measurements from our 1981 RGO Spectrograph spectrum of CPD – 56°8032. However, linewidths are not presented for the 1981 spectrum, because the instrumental profile dominated over the intrinsic Doppler widths of the nebular lines. Table 8 presents the line fluxes measured from our 1993 UCLES observations of He 2–113.

To obtain the nebular carbon abundance, we used the intensities of the C II] line at 2326 Å and of the C III] line at 1909 Å, measured from *IUE* spectra. Table 9 summarizes the *IUE* images that were used. For CPD – 56°8032, five different LWP frames (spectral range 1900–3200 Å) were averaged to improve the signal-to-noise ratio, while for He 2–113 only one LWP frame was found in the *IUE* archive. Four SWP frames (spectral range 1200–2000 Å) were used for CPD – 56°8032, while two were used for He 2–113. The region between 1800 and 2600 Å is displayed in Fig. 5 for both objects. As can be seen, the presence of the 2200-Å extinction feature does not allow us to locate the continuum accurately on the blue side of the 2326-Å feature, while it is somewhat easier to locate the continuum on both sides of the 1909-Å line. Due to the low signal-to-noise ratios, the flux and equivalent width measurements are affected by substantial uncertainties.

Table 8. Observed (F) and dereddened (I) nebular line intensities for He 2–113. The adopted reddening is $E(B-V)=1.00$. The dereddened Hβ flux is 6.12×10^{-11} erg cm^{-2} s^{-1}.

		He 2–113			
Ion	λ (Å)	FWHM (km s^{-1})	F (ergs cm^{-2} s^{-1})	100×I /I(Hβ)	Errors (%)
[O II]	3726.0	44	3.26×10^{-13}	15.1	20
[O II]	3728.8	47	1.42×10^{-13}	14.8	20
Hβ	4861.3	39	2.16×10^{-12}	100	10
[N II]	5754.6	40	2.42×10^{-13}	5.8	10
[O I]	6300.3	79	2.87×10^{-13}	5.2	10
[O I]	6363.8	69	1.02×10^{-13}	1.8	20
[N II]	6548.0	36	2.54×10^{-12}	40.5	10
Hα	6562.8	39	1.77×10^{-11}	281.1	10
[S II]	6716.5	42	1.78×10^{-13}	2.6	10
[S II]	6730.8	43	3.76×10^{-13}	5.5	20
[O II]	7320	–	1.43×10^{-12}	16.3	15
[O II]	7330	–	1.26×10^{-12}	14.3	15
O I	8445.5	39	3.04×10^{-13}	2.4	10
[Cl II]	8578.7	32	1.49×10^{-13}	1.1	10
[S III]	9068.9	29	1.02×10^{-12}	6.7	30

Table 9. Log of the *IUE* observations used to measure the intensity of the C II] 2326-Å and C III] 1909-Å lines.

Star	Frame	Exposure Time (min)
CPD–56°	LWP11203L	30
	LWP21065L	15
	LWP21076L	25
	LWR5733L	10
	LWR7700L	25
	SWP36663L	60
	SWP42316L	60
	SWP6718L	20
	SWP8947L	55
He 2–113	LWP21075L	90
	SWP8950L	40
	SWP42315L	180

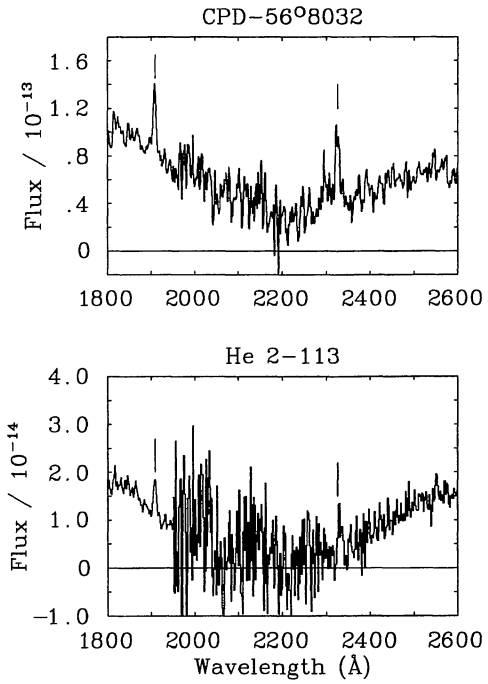

Figure 5. The C III] line at 1909 Å and the C II] line at 2326 Å, for CPD – 56°8032 (upper) and He 2–113 (lower). Fluxes are in erg cm^{-2} s^{-1} $Å^{-1}$.

In order to account for the stellar wind component contributing to the lines, we made use of the stellar wind equivalent widths predicted for the C II] λ2326 and C III] λ1909 features by our models (Paper II). For the λ2326 line, we obtained the equivalent width of the nebular component by subtracting the model prediction for the stellar wind equivalent width (21.1 Å for CPD – 56°8032 and 5.0 Å for He 2–113) from the total equivalent width of the 2326 Å feature as measured from the merged *IUE* spectra (35 Å for CPD – 56°8032 and 36 Å for He 2–113 respectively). We then scaled the model stellar continuum flux to the dereddened observed continuum flux at 5610 Å and measured this normalized model continuum flux at 2326 Å (9.99×10^{-12} and 2.04×10^{-11} erg cm^{-2} s^{-1} $Å^{-1}$ for CPD – 56°8032 and He 2–113 respectively), finally multiplying the derived nebular equivalent widths of 14 and 31 Å by these values. The result is equivalent to the dereddened flux arising from the nebular part of the λ2326 feature, and was found to be 1.40×10^{-10} erg cm^{-2} s^{-1} for CPD – 56°8032 and 6.32×10^{-10} erg cm^{-2} s^{-1} for He 2–113. For the C III] λ1909 feature, the measured equivalent widths of 6.8 Å for CPD – 56°8032 and 7.0 Å for He 2–113 are slightly smaller than (CPD – 56°8032) or equal to (He 2–113) the equivalent width predicted by the respective stellar wind model alone. We therefore conclude that there is no evidence for a significant nebular contribution to the observed C III] 1909-Å feature for either object.

The reason for using the stellar model continuum flux at 2326 Å and not the dereddened *IUE* continuum flux is that the accuracy of the latter is dependent on using the correct reddening law. The reddening law towards CPD – 56°8032 has previously been shown to be abnormal (Rao et al. 1990; Jeffery 1995) in the sense that the 2200-Å extinction feature is weak relative to the optical extinction. Confirming this, we found that dereddening the *IUE* spectra using the standard reddening law of Seaton (1979), with $E(B-V) = 0.68$ and 1.0 for CPD – 56°8032 and He 2–113, respectively, led to an overcorrection of the interstellar 2200-Å extinction feature. This can be attributed to part of the reddening to each object being circumstellar. Since the carbon-rich dust around these objects may not have the same reddening law as ISM dust, and since the UV is the region most sensitive to reddening-law variations, we therefore preferred to use our model stellar spectra, normalized to the dereddened optical spectra at 5610 Å, to estimate the dereddened stellar continuum flux at 2326 Å.

6.2 Nebular temperatures and densities

For both these objects, a nebular analysis is seriously hampered by the blending of stellar and nebular lines. Due to the fact that both nebulae are very compact, it was not possible to extract a clean nebular spectrum from the regions adjacent to the stellar spectrum.

Due to the richness of the stellar spectra, most nebular diagnostic lines are severely blended. The nebular [S II] λ6731 line is blended with a stellar wind C II multiplet 21 component (at 6731.1 Å) and with a stellar wind C III multiplet 3 component (at 6728.7 Å); the nebular [O II] 3726, 3729 Å doublet is blended with a stellar wind O II multiplet 3 component (at 3727.3 Å), while the [N II] nebular line at 5755 Å is partly blended with an O II multiplet 31.03 wind component at 5753.8 Å. This made it difficult to diagnose the nebular temperature and density in the usual way.

Due to the blending problem affecting the temperature-sensitive [N II] λ5755 line, we have chosen to use the four [O II] lines at 7318.8, 7319.9, 7329.6 and 7330.6 Å to estimate the nebular electron temperature in the following manner. The $^2P^0_{3/2}$ and $^2P^0_{1/2}$ levels from which the lines originate have high critical densities (between 4×10^6 and 6×10^6 cm^{-3}; Rubin 1989), so that their intensities are relatively insensitive to the nebular electron density, but their relatively high excitation energies make the lines temperature-sensitive.

The abundance of oxygen in PNe has been found to be not significantly altered by nucleosynthetic processes during

the evolution of the precursor star, as shown by a comparison with H II region oxygen abundances (Kingsburgh & Barlow 1994). We therefore adopted the mean O/H ratio of $(4.8 \pm 1.6) \times 10^{-4}$ derived by Kingsburgh & Barlow for a sample of 80 Galactic PNe as appropriate for the nebulae of CPD $-56°8032$ and He 2–113 as well. Since there is no doubly ionized oxygen in either nebula, we have that $O^+/H^+ = O/H$. Using the collision strengths and transition probabilities of Pradhan (1976) and Zeippen (1982), the dereddened [O II] $\lambda\lambda$7320, 7330/Hβ flux ratios in Tables 7 and 8 imply electron temperatures of 8800 and 9300 K for CPD $-56°8032$ (from our 1993 and 1981 spectra respectively) and 8400 K for He 2–113.

To estimate the errors on the derived temperatures, we calculated the temperatures corresponding to the limits on the mean PN O/H abundance stated by Kingsburgh & Barlow (1994): $O/H = (4.8 \pm 1.6) \times 10^{-4}$. In this way we found the nebular temperature limits of CPD $-56°8032$ to be 8800^{+600}_{-400} K (from our 1993 spectrum) and 9300^{+400}_{-600} K (from our 1981 spectrum), while for He 2–113 we obtained 8400^{+500}_{-300} K. We finally rounded the errors to ± 500 K for CPD $-56°8032$ and ± 400 K for He 2–113.

The discrepancy between the temperatures derived from the two different observations of CPD $-56°8032$ is due to the intensities, relative to Hβ, of the [O II] 7320, 7330 Å lines being greater in the 1981 observations than in the 1993 observations. The 1981 spectra had a lower resolution, and so measurements carried out on its blended 7320, 7330-Å lines are not as reliable as those carried out on the unblended features that appear in the 1993 spectrum. However, direct comparison of the 7300–7360 Å wavelength regions in the 1981 and 1993 spectra shows that, blending aside, the [O II] 7320, 7330-Å lines did appear to be stronger in 1981 than in 1993. In order not to exclude the possibility of changes having occurred in the intervening 12 years in the physical conditions of the nebula, we adopt the temperatures stated above to derive independent densities and abundances (see below in Section 6.3) from these two independent observations of CPD $-56°8032$.

To estimate the nebular electron densities, we have used the flux ratio of [O II] $\lambda\lambda$3726, 3729 to [O II] $\lambda\lambda$7320, 7330. The λ3726.0 and λ3728.8 lines, originating from $^2D^0_{5/2}$ and $^2D^0_{3/2}$ levels, have critical densities between 1×10^3 and 4×10^3 cm^{-3} (Rubin 1989). Thus, for electron densities lying between several thousand cm^{-3} and several million cm^{-3} (the latter being the critical densities of the $^2P^0$ levels from which the $\lambda\lambda$7320, 7330 lines originate), the [O II] λ3727/λ7325 flux ratio will be a sensitive density diagnostic. As shown in Figs 6 and 7, the λ3727/λ7325 ratio does have a weak sensitivity to the nebular electron temperature, but is primarily sensitive to the electron density within the observed range.

In the case of CPD $-56°8032$, the [O II] $\lambda\lambda$3726, 3729 complex was heavily blended with the stellar wind O II 3727.3 Å line, while for He 2–113 the narrower and weaker stellar wind line left the nebular [O II] lines uncontaminated. The O II 3727.3-Å line is the intermediate-strength component of a triplet whose other components are at 3712.7 and 3749.5 Å. In order to determine the flux due to the nebular lines alone, we measured the equivalent widths of the P Cygni emission and absorptions components of the O II stellar wind lines at 3712.7 and 3749.5 Å, and took an average of the sum of these emission and absorption equivalent widths to predict the O II λ3727.34 net emission contribution. We then measured the total equivalent width of the blend due to the nebular [O II] lines and the stellar wind O II line, and subtracted from it the predicted net stellar wind O II emission contribution. The nebular lines are estimated to contribute 70 per cent of the total flux in the blend. This procedure was followed with the 1993 spectrum of CPD $-56°8032$. However, for the 1981 spectrum the entire spectral region (3700–3750 Å) was crowded with emission lines, and the lower resolution could not distinguish the O II stellar wind features at 3712.7 and 3749.5 Å. This may be the main reason why the [O II] $\lambda\lambda$3726, 3729 fluxes from the 1981 spectrum are higher than those from the 1993 spectrum. However, if we use our 1993 result, i.e., that the nebular lines contribute 70 per cent to the blend, we obtain a nebular density which is less than 0.1 dex higher than that obtained by assuming that all of the flux is due to [O II]. This is within the error estimate and would only increase the resulting abundances by small amounts, well within the relative uncertainties.

The nebular electron densities derived from the dereddened [O II] 3727/7325 ratios (from Tables 7 and 8) are found to be $\log(N_e) = 4.8 \pm 0.1$ cm^{-3} for both the 1993 observation of CPD $-56°8032$, using $T_e = 8800 \pm 500$ K, and for the 1981 observation, using $T_e = 9300 \pm 500$ K. For He 2–113, we also obtained $\log(N_e) = 4.8 \pm 0.1$ cm^{-3} using $T_e = 8400 \pm 400$ K. The loci of the [O II] 7325/Hβ and [O II] 7325/3727 ratios in the $\log(N_e)$ versus T_e plane are plotted in Fig. 6 for CPD $-56°8032$ (1993; left) and CPD $-56°8032$ (1981; right), and in Fig. 7 for He 2–113. Also plotted for each nebula are the loci corresponding to the dereddened [N II] 6548/5755 ratios. These were calculated using the collision strengths and transition probabilities of Strafford et al. (1994) and Nussbaumer & Rusca (1979). In the case of the 1993 observation of CPD $-56°8032$, the [N II] ratio shows good consistency with the values of N_e and T_e given by the [O II] 7325/Hβ and [O II] 3727/7325 ratios, while for the 1981 observation, the [N II] ratio implies a density that is about 0.1 dex higher than given by the [O II] 3727/7325 ratio; in the case of He 2–113 the [N II] ratio implies an electron density which is 0.3 dex higher than given by the [O II] 3727/7325 ratio. Since, as mentioned above, the [N II] λ5755 line is potentially affected by serious line blending problems, we prefer to use the [O II] 7325/Hβ and [O II] 3727/7325 ratios as the electron temperature and density diagnostics. Overall, we prefer to base our conclusions about the nebula of CPD $-56°8032$ on the 1993 observations, because of their superior resolution.

The electron temperatures previously assumed for CPD $-56°8032$ were 10^4 K (Houziaux & Heck 1982: 'from the general appearance of the spectrum'; this was later adopted by Cohen et al. 1986) and 11 000 K (Rao 1987, who quotes the figure as an upper limit based on the presence of the [S III] lines at 9069 and 9532 Å). For He 2–113, Rao (1987) quotes 8800 K (from a comparison with a nebular analysis of SwSt 1 by Flower, Goharji & Cohen 1984, on the grounds that the nebulae are very similar). The nebular electron density for CPD $-56°8032$ was previously estimated to be 2×10^4 cm^{-3} (Rao 1987, from the ratio of the [N II] lines at 5755 and 6548 Å); Cohen et al. (1986) assumed it to be 1×10^4 cm^{-3}, from measurements on the

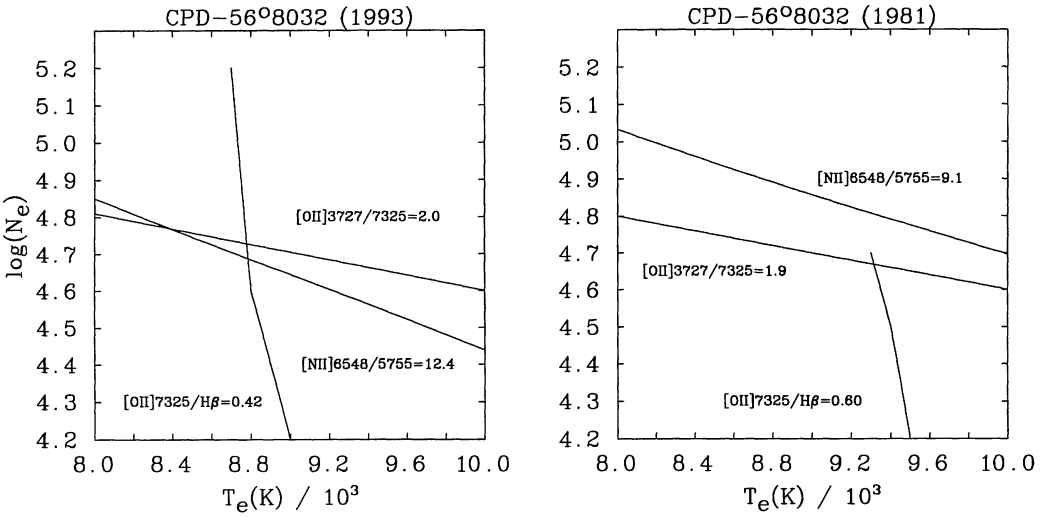

Figure 6. Diagnostic diagrams, $\log(N_e)$ versus T_e, for CPD – 56°8032 (1993) (left) and CPD – 56°8032 (1981) (right). The curves are based on the observed intensity ratios for [N II] 6548/5755; [O II] 3727/7325; and [O II] 7325/Hβ with the condition that the nebular O^+/H^+ ratio be equal to the mean PN O/H value of 4.8×10^{-4} found by Kingsburgh & Barlow (1994).

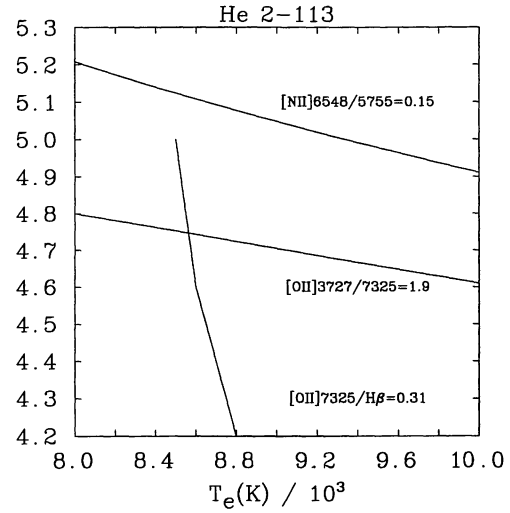

Figure 7. Diagnostic diagram, $\log(N_e)$ versus T_e, for He 2–113. The curves are bassed on the observed intensity ratios for [N II] 6548/5755; [O III] 3727/7325; and [O II] 7325/Hβ with the condition that the nebular O^+/H^+ ratio be equal to the mean PN O/H value of 4.8×10^{-4} found by Kingsburgh & Barlow (1994).

similar nebula M 4–18 by Goodrich & Dahari (1985). For He 2–113, Rao (1987) found 1×10^5 cm^{-3} from the [C I] $\lambda\lambda$8727, 9850 lines and a comparison with the spectrum of SwSt 1 (Flower et al. 1984). Our own nebular temperatures and densities are summarized in Table 10.

6.3 Nebular abundances

We have derived the nebular abundances of carbon, nitrogen and sulphur relative to hydrogen. The atomic collision strengths and transition probabilities for oxygen and nitrogen were discussed in Section 6.2. For S^+ we used collision strengths from Keenan et al. (1996) and transition probabilities from Mendoza & Zeippen (1982a) for S^{2+} the collision strengths were taken from Mendoza (1983), while the transition probabilities were taken from Mendoza & Zeippen (1982b). For C^+ we used collision strengths from Hayes & Nussbaumer (1984) and transition probabilities from Nussbaumer & Storey (1984).

Table 10. The electron temperatures and densities derived for the nebulae of CPD – 56°8032 and He 2–113.

Star	T_e(K)	$\log(N_e)$ (cm^{-3})
CPD–56°8032 (1993)	8800±500	4.8±0.1
CPD–56°8032 (1981)	9300±500	4.8±0.1
He 2–113	8400±400	4.8±0.1

As discussed in the previous section, oxygen was assumed to have the same abundance as the mean PN value of $(4.8 \pm 0.16) \times 10^{-4}$ found by Kingsburgh & Barlow (1994), in order to derive the electron temperature in the nebulae.

The nitrogen abundance was derived from the [N II] lines. The absence of the easily excited [O III] $\lambda\lambda$4959, 5007 lines in the spectra of these nebulae indicates the complete absence of O^{2+} ions. Although N^+ has a somewhat lower ionization potential than O^+ (29.6 versus 35.1 eV), we do not expect a significant abundance of N^{2+} ions to be present in the nebulae. We find that $N^+/H^+ = 1.0 \times 10^{-4}$ and 6.6×10^{-5} for CPD – 56°8032 and He 2–113 respectively. Both these values are below the mean PN value of 2.2×10^{-4}, but similar to the solar abundance of nitrogen derived from H II regions (Table 11). Due to his adoption of a high electron temperature of 11 000 K, Rao (1987) found lower values of N^+/H^+ for CPD – 56°8032 (1.4×10^{-5} and 5.2×10^{-5}, using the [N II] lines at 6548 and 5755 Å respectively).

S^+ has a lower ionization potential than either O^+ or N^+, and [S III] lines are observed in the spectra, at 3722, 9069

Table 11. Nebular abundances for CPD − 56°8032 and He 2–113. The abundances are by number. The lines used to derive the abundances are indicated in the header. Where more than one line is indicated a weighted average was taken. The C II] line flux was measured from *IUE* spectra (see Section 6.1). The high uncertainty in its measured flux is reflected in the C/H uncertainty. The mean PN abundances are from Kingsburgh & Barlow (1994); the solar O/H and S/H values are from Grevesse & Anders (1989); the solar N/H ratio is from Grevesse et al. (1990); and the solar C/H ratio is from Grevesse et al. (1991).

	C/H	O/H	N/H	S^+/H^+	S^{++}/H^+	S/H	C/O
	C II]	[O II]	[N II]	[S II]	[S III]		
λ (Å)	2326	7320,30	6548,5755	6717,6731	9068		
CPD–56°8032 (1993)	6.3±3.0(-3)*	4.8(-4)	8.3±0.8(-5)	1.0±0.1(-5)	3.9±1.0(-7)	1.0±0.1(-5)	13.1
CPD–56°8032 (1981)	7.2±3.0(-3)	4.7(-4)	1.0±0.1(-4)	1.3±0.1(-5)	–	1.3±0.1(-5)	15.3
He 2–113	5.0±3.0(-3)	4.8(-4)	6.6±0.7(-5)	2.6±0.3(-6)	1.3±0.1(-6)	3.9±0.5(-6)	10.4
Mean PN value	5.5±3.0(-4)	4.8±1.0(-4)	2.2±1.0(-4)	–	–	8.3±4.2(-6)	1.15
Solar	4.0±0.5(-4)	8.5±0.1(-4)	1.0±0.1(-4)	–	–	1.7±0.2(-5)	0.47

*$6.3 \pm 3.0(-3) = (6.3 \pm 3.0) \times 10^{-3}$.

and 9532 Å. Only the 9069-Å line was measured, as it was inferred not to be significantly affected by water vapour absorption in the Earth's atmosphere. The rest wavelength of the [S III] 9069-Å line is 9068.9 Å (Osterbrock, Tran & Veilleux 1992), while the only water vapour line that could affect the feature has a rest wavelength of 9069.126 Å. For both nebulae, the [S III] feature is blueshifted by approximately 1.8 Å, corresponding to the nebular radial velocities of 60 km s^{-1}. Thus the nebular [S III] λ9069 line is shifted away from the water vapour line, and its flux should not be depleted. For CPD − 56°8032 we obtain $S/H = 1.2 \times 10^{-5}$ from the sum of the S^+ and S^{2+} abundances (Table 11), while for He 2–113 we obtain $S/H = 3.8 \times 10^{-6}$. These sulphur abundances agree with the mean PN value of 8.3×10^{-6} within the uncertainties (see Table 11).

The nebular carbon abundance is given directly by the abundance of C^+ since, as explained in Section 6.1, we consider the C III] line at 1909 Å to have a stellar wind origin. We obtain $C/H = 6.3 \times 10^{-3}$ for CPD − 56°8032 and 5.0×10^{-3} for He 2–113. These carbon abundances are much higher than the mean PN value of 5.5×10^{-4} found by Kingsburgh & Barlow (1994), which may indicate that the inner (ionized) nebulae of these two objects have been contaminated by the carbon-rich stellar winds.

For CPD − 56°8032 we can reconcile our C^+/H^+ ratio with the lower ratios derived by Houziaux & Heck (1982) andf Cohen et al. (1989) on the grounds of our higher $I(\lambda 2326)/I(H\beta)$ and of our lower electron temperature (8800 K versus their adopted 10 000 K).

No nebular He^+ recombination lines are detected in our spectra. Our claim that the He I lines in the spectra of CPD − 56°8032 and He 2–113 are entirely of stellar origin is based on their profiles. However, the P Cygni nature of the stellar wind He I lines could make it extremely difficult to detect a weak nebular component added to the stellar feature, so that we cannot exclude the presence of some He^+ in the nebula. Table 11 summarizes our derived nebular abundances for both objects.

7 DISCUSSION

The very high C/O number ratios derived from the ionized zone around CPD − 56°8032 and He 2–113 (13 and 10 respectively; Table 11) confirms the strong correlation found by Cohen et al. (1989) between the C/O ratio and the ratio of UIR-band flux to total infrared flux – these two objects had by far the highest ratios of UIR to total infrared flux in their sample. Although their C/O ratios are very much higher than usually found for Galactic PNe, they are not unprecedented – the PN K648 in the globular cluster M15 has C/O = 8 (Howard, Henry & McCartney 1997), while the Galactic halo PN H 4–1 and BB-1 have C/O ratios of 10 and 13 respectively (Clegg 1989; Howard et al. 1997).

It has been suggested that [WCL] stars evolve into [WCE] stars and subsequently become PG1159-type white dwarfs (e.g. Barlow & Storey 1993; Leuenhagen et al. 1994). According to what we shall call the 'standard scenario' the [WC] central stars originate from AGB giants, with their hydrogen deficiency being caused by the almost complete removal of their hydrogen envelopes, perhaps due to a thermal pulse at the end of the AGB phase.

An alternative scenario conceives of some WR central stars as descending from a hydrogen-rich CSPN which experienced a final helium thermonuclear runaway pulse when it had already become a white dwarf (Schönberner 1979; Iben et al. 1983). Such a star would then return to the top of the AGB to complete another excursion, this time as a helium-burner with a new, hydrogen-deficient PN around it. This latter scenario resolved some discrepancies in the abundances seen in PNe such as Abell 30 and 78; amongst other things, it has also been seen as a possible solution to the mystery of the origin of R Coronae Borealis stars (hydrogen-deficient stars, only rarely associated with a PN).

The hydrogen-rich outer nebulae around Abell 30 and 78 have very low electron densities and surface brightnesses, consistent with having been ejected a considerable time ago, whereas their inner nebular knots, attributed by Iben et al. (1983) to ejecta from a final helium-shell flash on the white dwarf track that caused the stars to briefly return to the AGB, are helium-rich and lack any hydrogen (Hazard et al. 1980). By contrast, the high electron densities of the hydrogen-rich nebulae around CPD − 56°8032 and He 2–113 (6×10^4 cm^{-3}) appear consistent with both objects having recently left the AGB and transited to the PN phase

according to the standard scenario. Although the inner nebulosity carbon abundances are enhanced with respect to the mean PN value, this could, however, be the result of contamination of the nebular material by the WR wind.

Since the material around both the objects considered in this paper is unlikely to be fully ionized, due to the low effective temperatures of the stars (the strong observed CO emission supports this interpretation), we cannot conclude anything as to the overall outer dimensions and dynamical ages of the circumstellar material from the *HST* observations (what we see in Figs 3 and 4 is only the ionized part of the nebulae – neutral gas could be present outside that region extending up to several times the ionized regions). However, the apparent expansion age of CPD – 56°8032's inner ring of nebular emission is only 100 yr, which could give us some idea as to when the nebular ejection *terminated*.

In conclusion, we can say that these two stars are most likely to be objects that have evolved from the AGB according to the standard scenario. A few questions remain, which will have to await resolved nebular spectroscopy and deeper images.

ACKNOWLEDGMENTS

We thank Dr P. A. Crowther for useful comments. Dr J. R. Deacon is thanked for the filter profiles and calibrations that enabled us to derive broad-band magnitudes from our spectrophotometry. We are grateful to Dr W. Lawson and A. Jones for providing the latest light curves for both CPD – 56°8032 and He 2–113. OD acknowledges financial support from the Perren Fund during the period of this research. Finally, we acknowledge the useful comments of the referee.

REFERENCES

Aitken D. K., Barlow M. J., Roche P. F., Spencer P. M., 1980, MNRAS, 192, 679
Barlow M. J., 1983, in Flower D. R., ed., Proc. IAU Symp. 103, Planetary Nebulae. Reidel, Dordrecht, p. 105
Barlow M. J., Storey P. J., 1993, in Weinberger R., Acker A., eds, Proc. IAU Symp. 155, Planetary Nebulae. Kluwer, Dordrecht, p. 92
Bidelman W. P., MacConnell D. J., Bond H. E., 1968, IAU Circ. 2089
Brand J., Blitz L., 1993, A&A, 275, 67
Carlson E. D., Henize K. G., 1979, Vistas Astron., 23, 213
Clayton G. C., 1996, PASP, 108, 225
Clegg R. E. S., 1989, in Torres-Peimbert S., ed., Proc. IAU Symp. 131, Planetary Nebulae. Kluwer, Dordrecht, p. 139
Cohen M., Barlow M. J., 1980, ApJ, 238, 585
Cohen M., Allamandola L. J., Tielens A. G. G. M., Bregman J., Simpson J. P., Witteborn F. C., Wooden D., Rank D., 1986, ApJ, 302, 737
Cohen M., Tielens A. G. G. M., Bregman J. D., Witteborn F. C., Rank D. M., Allamandola L. J., Wooden D. H., de Muizon M., 1989, ApJ, 341, 246
Cowley A. P., Hiltner W. A., 1969, A&A, 3, 372
Crowther P. A., De Marco O., Barlow M. J., 1997, submitted
De Marco O., 1993, BSc Project dissertation, Univ. London
De Marco O., Crowther P. A., 1997, submitted (Paper II)
De Marco O., Storey P. J., Barlow M. J., 1997, submitted (Paper III)
Dinerstein H. L., Sneden C., Uglum J., 1995, ApJS, 447, 262
Fich M., Blitz L., Stark A. A., 1989, ApJ, 342, 272
Flower D. R., Goharji A., Cohen M., 1984, MNRAS, 206, 293
Goodrich R. W., Dahari O., 1985, ApJ, 289, 342
Grevesse N., Anders A., 1989, in Waddington C. J., ed., AIP Conf. Proc. 183, Cosmic Abundances of Matter. Am. Inst. Phys., New York, p. 1
Grevesse N., Lambert D. L., Sauval A. J., van Dishoeck E. F., Farmer C. B., Norton R. H., 1990, A&A, 232, 225
Grevesse N., Lambert D. L., Sauval A. J., van Dishoeck E. F., Farmer C. B., Norton R. H., 1991, A&A, 242, 488
Hayes M. A., Nussbaumer H., 1984, A&A, 134, 194
Hazard C., Terlevich R., Ferland G., Morton D. C., Sargent W. L., 1980, Nat, 285, 243
Hernize K. G., 1967, ApJS, 14, 125
Hillier D. J., 1990, A&A, 231, 111
Houziaux L., Heck A., 1982, in de Loore C. W. H., Willis A. J., eds, Proc. IAU Symp. 99, Wolf–Rayet Stars: Observations, Physics, Evolution. Reidel, Dordrecht, p. 139
Howard J. W., Henry R. B. C., McCartney S., 1997, MNRAS, 284, 465
Howarth I. D., 1983, MNRAS, 203, 301
Howarth I. D., Murray J., 1988, Starlink User Note No. 50
Humphreys R. M., 1978, ApJS, 38, 309
Iben I., Jr, Kaler J. B., Truran J. W., Renzini A., 1983, ApJ, 264, 605
Jeffery C. S., 1995, A&A, 299, 135
Keenan F. P., Aller L. H., Bell K. L., Hyung S., McKenna F. C., Ramsbottom C. A., 1996, MNRAS, 281, 1073
Kingsburgh R. L., Barlow M. J., 1994, MNRAS, 271, 257
Kohoutek L., 1996, in Jeffery C. S., Heber U., eds, ASP Conf. Ser. 96: Hydrogen-deficient Stars. Astron. Soc. Pac., San Francisco, p. 219
Lawson W. A., Jones A. F., 1992, Observatory, 112, 231
Lawson W. A., Jones A. F., 1996, in Jeffery C. S., Heber U., eds, ASP Conf. Ser. 96: Hydrogen-deficient Stars. Astron Soc. Pac., San Francisco, p. 151
Le Bertre T., Epchtein N., Gouiffes C., Heydari-Malayeri M., Perrier C., 1989, A&A, 225, 417
Leuenhagen U., Heber U., Jeffery C. S., 1994, A&A, 283, 567
Lynds B. T., 1980, AJ, 85, 1046
Mendez R., 1982, in de Loore C. W. H., Willis A. J., eds, Proc. IAU Symp. 99: Wolf–Rayet Stars: Observations, Physics, Evolution. Reidel, Dordrecht, p. 457
Mendoza C., 1983, in Flower D. R., ed., Proc. IAU Symp. 103, Planetary Nebulae. Reidel, Dordrecht, p. 143
Mendoza C., Zeippen C. J., 1982a, MNRAS, 198, 127
Mendoza C., Zeippen C. J., 1982b, MNRAS, 199, 1025
Milne D. K., Aller L. H., 1975, A&A, 38, 183
Nussbaumer H., Rusca C., 1979, A&A, 72, 129
Nussbaumer H., Storey P. J., 1984, A&AS, 56, 293
Oke J. B., 1974, ApJS, 27, 21
Oke J. B., 1990, AJ, 99, 1621
Osterbrock D. H., Tran H. D., Veilleux S., 1992, ApJ, 389, 305
Pollacco D. L., Kilkenny D., Marang F., Van Wyk F., Roberts G., 1992, MNRAS, 256, 669
Pradhan A. K., 1976, MNRAS, 177, 31
Purton C. R., Fedelman P. A., Marsh K. A., Allen D. A., Wright A. E., 1982, MNRAS, 1908, 321P
Rao N. K., 1987, QJRAS, 28, 261
Rao N. K., Giridhar S., Nandy K., 1990, A&A, 234, 410
Roche P. F., Allen D. A., Bailey J. A., 1986, MNRAS, 220, 7P
Rubin R. H., 1989, ApJS, 69, 897
Sahai R., Wootten A., Clegg R. E. S., 1993, in Weinberger R., Acker A., eds, Proc. IAU Symp. 155: Planetary Nebulae. Reidel, Dordrecht, p. 229

Schönberner D., 1979, A&A, 79, 108
Seaton M. J., 1979, MNRAS, 187, 73
Shull J. M., Van Steenberg M. E., 1985, ApJ, 294, 559
Smith L. F., 1968, MNRAS, 138, 109
Snyder D. L., 1990, in White R. L., Allen R. J., eds, The Restoration of *HST* Images and Spectra. STScI, Baltimore, p. 56
Storey P. J., Hummer D. G., 1995, MNRAS, 272, 41
Strafford R. P., Bell K. L., Hibbert A., Wijesundera W. P., 1994, MNRAS, 268, 816
Swings P., Struve O., 1940, Proc. Nat. Acad. Sci., 26, 454
Thackeray A. D., 1977, Observatory, 07, 165
Tylenda R., Acker A., Stenholm B., 1993, A&AS, 102, 595
van der Hucht K. A., Conti P. S., Lundstrom I., Stenholm B., 1981, Space Sci. Rev., 28, 227
Vassiliadis E., Wood P. R., 1994, ApJS, 92, 125
Walton N. A., Pottasch S. R., Reay N. K., Taylor A. R., 1988, A&A, 200, 21L
Webster B. L., Glass I. S., 1974, MNRAS, 166, 491
Zeippen C. J., 1982, MNRAS, 198, 111

APPENDIX A: DISTANCES FROM A MAGELLANIC CLOUD LUMINOSITY CALIBRATION

The distance to each star was estimated using two different methods. The first method uses the fact that effectively all the bolometric luminosity of CPD – 56°8032 and He 2–113 is reradiated in the infrared by cool dust (Aitken et al. 1980). To obtain the bolometric luminosities, we made use of the 1–3.5 μm photometry of Webster & Glass (1974), the 3.5–20 μm photometry of Cohen & Barlow (1980), the mean 7–22 μm *IRAS* LRS spectrum and the (colour-corrected) *IRAS* Point Source Catalogue 12–100 μm fluxes. We derived an infrared bolometric luminosity of 2820 D^2 $L_\odot$ for CPD – 56°8032 and 2290 D^2 $L_\odot$ for He 2–113 (where D is the distance in kpc), using the measured integrated infrared fluxes of 9.01×10^{-15} and 7.32×10^{-15} W cm^{-2} respectively.

We can estimate the distances to the stars by using WR central stars of Magellanic Cloud PNe as calibrators, since they have known distances. Dr X.-W. Liu (private communication) analysed five Magellanic Cloud PNe having WR nuclei and obtained a mean central star mass of 0.62 ± 0.02 $M_\odot$ from a comparison of the derived effective temperatures and luminosities with Vassiliadis & Wood (1994) helium-burning evolutionary tracks. This mean mass was assumed for our two stars (since neither star has any hydrogen in its envelope, they must both be on helium-burning tracks). The Vassiliadis & Wood helium-burning tracks were then applied to predict the luminosity for central stars of this mean mass having effective temperatures of 30 000 and 30 900 K (derived in Paper II for CPD – 56°8032 and He 2–113 respectively).[4] The predicted luminosity is 5100 $L_\odot$ for both stars (because the tracks were calculated only for stars of mass 0.600 ot 0.634 $M_\odot$, we interpolated to obtain the luminosities corresponding to 0.62 $M_\odot$). The distance established in this way for CPD – 56°8032 was 1.35 kpc, while for He 2–113 we derived a distance of 1.50 kpc. Our error estimate of ± 0.3 kpc is based on two factors. First, uncertainties in the IR flux estimate arise from the fact that, longwards of 20 μm, only three *IRAS* points are available and so the interpolation is affected by a corresponding uncertainty. Secondly, errors may be associated with using helium-burning tracks calculated for stars with hydrogen-rich envelopes and assuming them to apply to WR central stars which lack any hydrogen.

[4]The effective temperatures were derived from our modelling of the stellar winds using the codes written by D. J. Hillier (1990) – see Paper II. We note that a change of 10 000 K in the adopted effective temperature changes the derived distance by only 5 per cent.

APPENDIX B: GALACTIC ROTATION CURVE DISTANCES

An independent estimate for the distance to each of the stars comes from the Na I D interstellar absorption lines. Fig. B1 shows the wavelength range between 5880 and 5900 Å, dominated by emission due to the $3d\,^2D$–$4p\,^2P^0$ multiplet 5 of C II. Superimposed on this feature is absorption due to the sodium D1 and D2 lines corresponding to a number of radial velocity components: some of interstellar origin, and some related to the material around the stars (see below). LSR radial velocities of these absorption components were measured for both the D lines and are tabulated in Table 3, along with the LSR radial velocity of the nebulae obtained from the Balmer lines. The Na I measurements were carried out by fitting a multiple-cloud model to the data (where the number of components, their internal velocity dispersions and the column densities were free parameters), after the C II emission profile was rectified. The rectification was achieved by fitting two Gaussians to

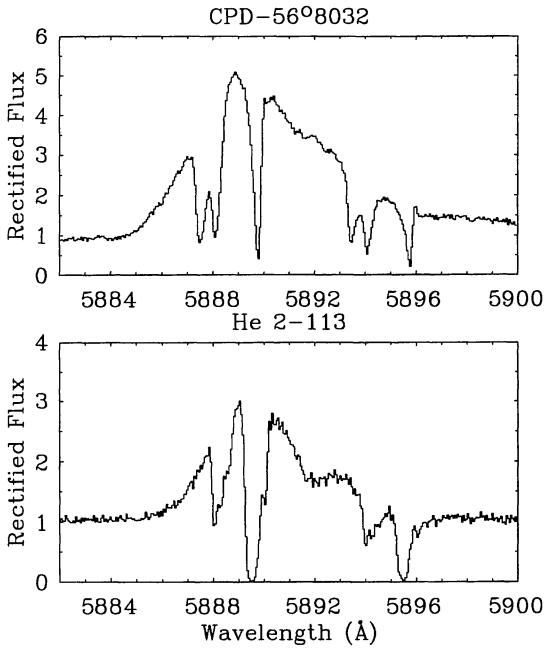

Figure B1. The sodium D region in the spectra of CPD – 56°8032 (upper) and He 2–113 (lower). The emission is due to C II multiplet 5, while the absorption lines are due to the sodium D1 and D2 lines at 5895.924 and 5889.950 Å, which exhibit a number of radial velocity components.

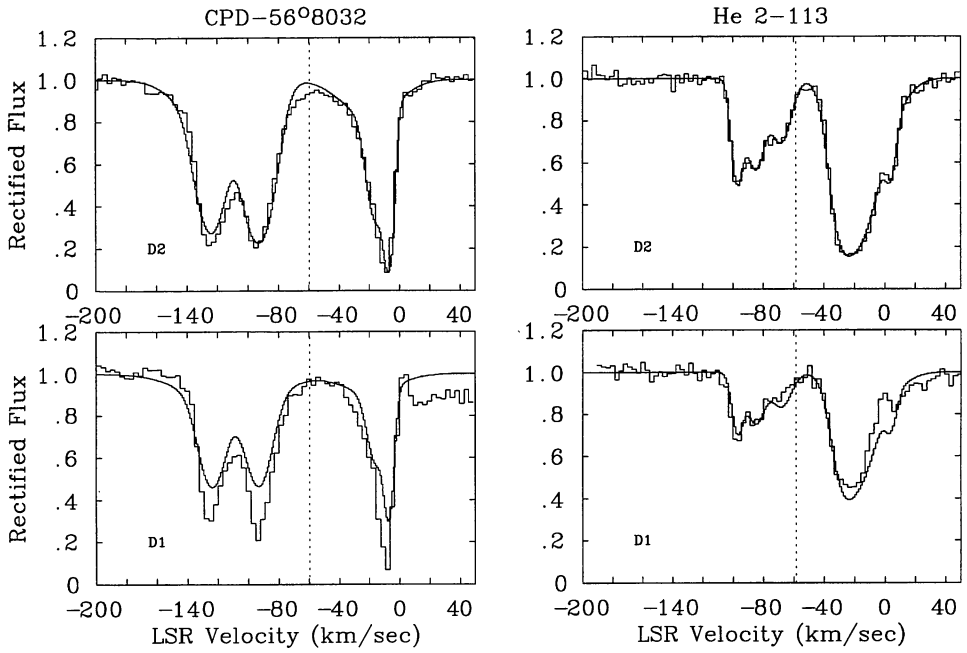

Figure B2. The rectified Na I D line profiles for CPD – 56°8032 and He 2–113. The LSR radial velocity of each star is marked by the vertical dotted line.

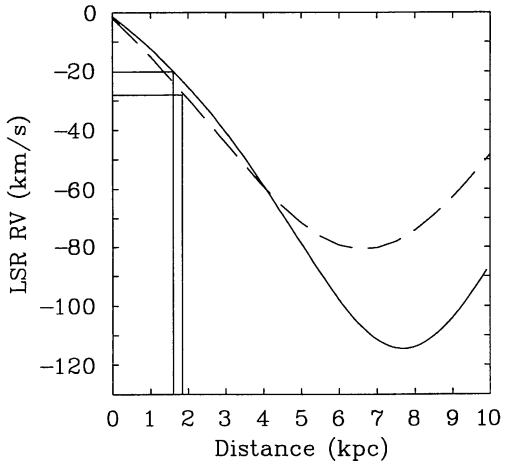

Figure B3. Galactic rotation curves for the directions towards CPD – 56°8032 (solid) and He 2–113 (dashed), as predicted by the model of Brand & Blitz (1993).

the emission lines. Fits with more than two Gaussians did not rectify the profiles satisfactorily, although we recognize the possibility of other weaker emission lines being present in the region. We fitted the sodium D2 absorption line (see Fig. B2), which has the better signal-to-noise ratio, and then the D1 line with the same cloud parameters, to make sure that the components matched. The D1 fits are not as good as the D2 fits, mainly because of imperfect rectification of the emission profiles, but it is apparent that the positions of the velocity components match.

If interstellar sodium were homogeneously distributed, we would expect to find a wide Na I absorption feature extending from zero radial velocity up to the LSR radial velocity of material near to the star. Use of the Galactic rotation curve for a particular line of sight would then allow us to derive the distance to the star. The obvious limitations of this method are the inhomogeneity of the ISM, so that we cannot be sure that absorbing material extends all the way to the star (this means that we will really only measure a lower limit to the distance) and uncertainties associated with the adopted rotation curve. Moreover, in the case of PNe, there is the further problem that Na I may be present within the neutral envelope surrounding the nebula, causing absorption features at radial velocities corresponding to the nebular expansion velocity (e.g. Dinerstein, Sneden & Uglum 1995; see Section 3.4).

We adopted the rotation curve of Brand & Blitz (1993) with $R_0 = 8.5$ kpc and $\theta_0 = 220$ km s^{-1}, which yields almost identical results to that of Fich, Blitz & Stark (1989). The Galactic rotation curves corresponding to the directions towards CPD – 56°8032 ($l = 332.^{\circ}92$, $b = -9.^{\circ}91$) and He 2–113 ($l = 321.^{\circ}05$, $b = 3.^{\circ}99$) are plotted in Fig. B3.

We cannot assume that all of the velocity components in Fig. B2 are of interstellar origin. Interstellar gas in the line of sight should move towards us at velocities more positive than -80 km s^{-1} for He 2–113, and more positive than -110 km s^{-1} for CPD – 56°8032 (cf. Fig. B3). In addition, for both sightlines we should not expect to find *interstellar* material at velocities more negative than the objects radial velocity. In Fig. B2 the nebular radial velocities (derived from the Balmer lines) are marked by the vertical dotted lines. We interpret velocity components which are at more negative velocities than these as arising from expanding circumnebular neutral gas in front of the stars. If we confine our attention to less negative velocities than the nebular radial velocity, then for CPD – 56°8032 the most negative (interstellar) velocity component is at -20 km s^{-1}, while for He 2–113 the most negative component is at -29 km s^{-1}. From Fig. B3, these velocities imply distances of

1.6 ± 0.2 kpc for CPD $-56°8032$ and 1.9 ± 0.2 kpc for He 2–113. These values agree, within the relative uncertainties, with the respective distances of 1.35 ± 0.3 and 1.50 ± 0.3 kpc obtained from the Magellanic Cloud [WC] star luminosity calibration.

If we assume that the scaleheight of interstellar Na I is closely related to that of neutral hydrogen (144 ± 80 pc, Shull & Van Steenberg 1985; 197 ± 29 pc, De Marco 1993), then the rotation curve distance of 1.9 kpc for He 2–113 would put it at a height of 132 pc above the Galactic plane, comfortably within a H I scaleheight, while for CPD $-56°8032$ the implied distance of 1.6 kpc would put it 275 pc below the plane, a little below the H I scaleheight of 197 pc found by De Marco (1993). Both distance methods comfortably position both nebulae within the Sagittarius arm of the Galaxy (Lynds 1980; Humphreys 1978).